Metabolic Brain Disease (2018) 33:1661–1668
https://doi.org/10.1007/s11011-018-0274-7

ORIGINAL ARTICLE

Metabolic fate of glucose in the brain of APP/PS1 transgenic mice at 10 months of age: a ^{13}C NMR metabolomic study

Qi Zhou[1] · Hong Zheng[1] · Jiuxia Chen[1] · Chen Li[1] · Yao Du[1] · Huanhuan Xia[1] · Hongchang Gao[1]

Received: 18 January 2018 / Accepted: 19 June 2018 / Published online: 26 June 2018

Abstract

Alzheimer's disease (AD) has been associated with the disturbance of brain glucose metabolism. The present study investigates brain glucose metabolism using ^{13}C NMR metabolomics in combination with intravenous [1-^{13}C]-glucose infusion in APP/PS1 transgenic mouse model of amyloid pathology at 10 months of age. We found that brain glucose was significantly accumulated in APP/PS1 mice relative to wild-type (WT) mice. Reductions in ^{13}C fluxes into the specific carbon sites of tricarboxylic acid (TCA) intermediate (succinate) as well as neurotransmitters (glutamate, glutamine, γ-aminobutyric acid and aspartate) from [1-^{13}C]-glucose were also detected in the brain of APP/PS1 mice. In addition, our results reveal that the ^{13}C-enrichments of the C3 of alanine were significantly lower and the C3 of lactate have a tendency to be lower in the brain of APP/PS1 mice than WT mice. Taken together, the development of amyloid pathology could cause a reduction in glucose utilization and further result in decreases in energy and neurotransmitter metabolism as well as the lactate-alanine shuttle in the brain.

Keywords ^{13}C flux · Energy metabolism · Brain glucose · Neurodegenerative disease · Neurotransmitter

Abbreviations

AD	Alzheimer's disease
Ala	Alanine
Asp	Aspartate
^{13}C-NMR	^{13}C nuclear magnetic resonance
GABA	γ-aminobutyric acid
Glu	Glutamate
Gln	Glutamine
Lac	Lactate
MWM	Morris water maze
PC	Pyruvate carboxylase
PDH	Pyruvate dehydrogenase
Suc	Succinate
T1D	Type 1 diabetes
T2D	Type 2 diabetes
TCA	Tricarboxylic acid
WT	Wild-type

Qi Zhou and Hong Zheng contributed equally to this work.

✉ Hong Zheng
123zhenghong321@163.com

✉ Hongchang Gao
gaohc27@wmu.edu.cn

[1] Institute of Metabonomics & Medical NMR, School of Pharmaceutical Science, Wenzhou Medical University, Wenzhou 325035, China

Introduction

Alzheimer's disease (AD) is a chronic neurodegenerative disease characterized by amyloid plaques and neurofibrillary tangles (Blennow et al. 2006; Hardy and Selkoe 2002). AD is also a leading cause of dementia with an estimated prevalence of 42.3 million people worldwide in 2020 (Ferri et al. 2005), which seriously impair quality of life in AD patients. Moreover, this number will be increased to 81.1 million by 2040 (Ferri et al. 2005). Even more unfortunate is the fact that currently there is no effective strategy to treat or delay the development of AD (Hardy and Selkoe 2002; Holtzman et al. 2011). Therefore, further exploring the pathogenesis of AD will advance the development of clinical treatments for AD.

Although many factors involved in AD pathogenesis, the major cause is amyloid β (Aβ) deposition which results in brain neuronal dysfunction and apoptosis (Ferri et al. 2005). In addition, AD has also been implicated in metabolic disorders including glucose homeostasis and energy metabolism (Suzanne 2014). A stable energy metabolism is essential for

keeping normal brain function. The brain possesses only 2% of the total body mass, but about 25% of glucose in the brain is metabolized for energy production (Bélanger et al. 2011). Moreover, brain glucose metabolism produces a series of metabolic intermediates including neurotransmitters and thereby maintains normal brain metabolism (Hoyer et al. 1996). Therefore, brain glucose hypometabolism has been implicated in the progression of AD (Mosconi 2005). Results from positron emission tomography and magnetic resonance imaging studies have shown that the disturbance of brain glucose metabolism can be regarded as an indicator of neuronal dysfunction in AD patients (Saint-Aubert et al. 2016; Li et al. 2016; Ballarini et al. 2016; Winkler et al. 2015). However, the detailed characteristics on brain glucose metabolism in AD are still far from being fully understood.

^{13}C nuclear magnetic resonance (NMR) technique is a promising tool to track metabolic fate related to a specific metabolite (Shulman et al. 1990; Sibson et al. 2001; Zwingmann et al. 2003). The change of ^{13}C incorporation from ^{13}C-labelled substrate into other metabolites can be monitored by using ^{13}C-NMR spectroscopy. In our previous study, a ^{13}C NMR metabolomic approach in combination with intravenous [1-^{13}C]-glucose and [2-^{13}C]-acetate infusions was used to explore the changes in brain energy metabolism during type 1 diabetes (T1D) development (Wang et al. 2015). We found that mitochondrial metabolism was enhanced in astrocytes but impaired in neurons (Wang et al. 2015). Furthermore, we used ^{13}C NMR metabolomics with [2-^{13}C]-acetate and [3-^{13}C]-lactate infusions to explore neuronal and astrocytic metabolism in the brain of *db/db* mice (Zheng et al. 2017). Our results showed that an unbalanced metabolic cooperation between astrocyte and neuron as well as an enhanced gluconeogenesis in type 2 diabetic (T2D) mice with cognitive decline (Zheng et al. 2017). The aim of the present study was to explore glucose metabolism in the brain of APP/PS1 transgenic AD mice at 10 months of age using a ^{13}C NMR metabolomic approach in combination with intravenous [1-^{13}C]-glucose infusion. This study will provide valuable information to further investigate the potential brain metabolic mechanism of amyloid pathology.

Materials and methods

Animals

Four-week-old APP/PS1 double transgenic mice (male, body weight = 23.7 ± 1.6 g, n = 7) and wild-type mice (male, body weight = 25.7 ± 2.3 g, n = 7) were purchased from the Mode Animal Research Center of Nanjing University (Nanjing, China) and housed in the Experimental Animal Center of Wenzhou Medical University (Wenzhou, China). During the whole feeding process, all mice had free access to standard rat chow and tap water in a specific pathogen-free colony with regulated temperature and humidity under a 12:12 h light:dark cycle. All animal experiments were performed in accordance with the Guide for the Care and Use of Laboratory Animals and approved by the Institutional Animal Care and Use Committee of Wenzhou Medical University. Experiments were reported according to the ARRIVE guidelines.

Morris water maze (MWM) test

The MWM test was conducted to evaluate the performance of spatial learning and memory in mice, as described in our previous study (Zheng et al. 2017). Briefly, the MWM test was performed using a circular pool (diameter = 110 cm; height = 30 cm) filled with opaque water at 26 ± 1 °C. The escape platform with a diameter of 7 cm was submerged 1 cm below the surface of the water. During the training period, if mice cannot find the escape platform within 60 s, the experimenter guided them to reach the escape platform. The training period continued for 4 days and 4 trials per day. After this period, the escape platform was removed, and mice were subjected to a 60s probe test at the same start location. The behavior of mice was tracked and recorded using an overhead video camera. The escape latency, the number of crossings over the original platform location as well as the percentages of swimming length and time in the goal area were calculated by a computer system equipped with 'Viewer 2' software (Biobserve GmbH, Bonn, Germany).

Intravenous [1-^{13}C]-glucose infusion

APP/PS1 and WT mice at 10 months of age were anesthetized with chloral hydrate after overnight fasting prior to operation. The glow lamp was used to maintain the rectal temperature of mice at 36.8–37.5 °C. [1-^{13}C]-glucose (Sigma-Aldrich, > 99% pure) was prepared in normal saline at a concentration of 0.5 mol/l and then continuously injected through left jugular veins with a micro syringe pump at the rate of 0.1 ml/kg/min for 30 min. For a ^{13}C NMR analysis, a substantial amount of samples was required to acquire sufficient sensitive signals due to the low abundance of ^{13}C. After 15 min of infusion, therefore, the whole brain was taken out immediately and frozen in liquid nitrogen. The level of blood glucose in mice before and after injection [1-^{13}C]-glucose was measured from a tail nick by a handheld glucometer (B/BRAUN omnitest plus).

^{13}C nuclear magnetic resonance analysis

The brain tissue was extracted using the methanol–chloroform method as described previously (Wang et al. 2015). In brief, the brain tissue was weighed into a centrifuge tube and added with ice-cold methanol (4.0 ml/g) as well as distilled water

(2.0 ml/g). The mixture was homogenized and mixed by vortex at 4 °C. Then, ice-cold chloroform (2.0 ml/g) and distilled water (2.0 ml/g) were added into the mixture, mixed again and allowed to stand for 15 min on ice. After centrifugation at 1000 g for 15 min, the supernatant was transferred into a new centrifuge tube, lyophilized for about 24 h and stored at -80 °C until use. The lyophilized sample was reconstituted with 0.6 ml of D_2O (99.5%) containing 0.05% of sodium trimethlysilyl propionate-d_4 (TSP) and transferred to a 5 mm NMR tube for NMR analysis.

^{13}C NMR spectra were recorded at 298 K on a Bruker AVANCE III 600 MHz NMR instrument at 150.92 MHz, using an inverse-gated decoupling sequence to avoid the nuclear overhauser effect. The main parameters were set as follows: flip angle = 30°; relaxation delay = 2 s; spectral width = 33,333 Hz; scan number = 16,384; acquisition time = 1 s; data points = 64 K. NMR metabolic signals were assigned in accordance with our published data (Wang et al. 2015). The specific ^{13}C-enrichment of metabolites after [1-^{13}C]-glucose infusion was calculated assuming that the natural abundance of ^{13}C is 1.1%.

Data analysis

In this study, all mice were randomly assigned to the experimental procedures, such as housing and feeding, the MWM test, animal operation as well as sample collection. NMR metabolomic analysis was conducted by masking animal group labels. The difference in metabolic and behavior data between APP/PS1 and WT mice was analyzed by Student's t test in SPSS software (version 13.0, SPSS Inc., Chicago, IL, USA). The difference with a P value <0.05 was considered to be statistically significant.

Results

Learning and memory performance in APP/PS1 mice

Results from the MWM test of APP/PS1 and WT mice at 10 months of age are shown in Fig. 1. We found that the escape latency was remarkably longer in APP/PS1 mice at 10 months of age than age-matched WT mice on day 3 and day 4 as shown in Fig. 1a. The swimming path of WT and APP/PS1 mice at 10 months of age are illustrated in Fig. 1b. The percentage of total swimming length and time in the target quadrant as well as the number of crossings over the original platform location during the probe trial were shown in Fig. 1c–e, respectively. We can see that these behavioral parameters were significantly lower in APP/PS1 mice than in WT mice. Taken together, the MWM test demonstrates that learning and memory ability was impaired in APP/PS1 mice at 10 months of age.

Metabolic changes in the brain of APP/PS1 and WT mice after [1-^{13}C]-glucose infusion

Figure 2a, b show typical ^{13}C NMR spectra of brain tissue samples in APP/PS1 and WT mice at 10 months of age after [1-^{13}C]-glucose infusion, respectively. It can be seen from ^{13}C NMR spectra that ^{13}C isotope of [1-^{13}C]-glucose has been incorporated into the specific carbon sites of metabolites, including glutamate (Glu: C2, δ55.7; C3, δ28; C4, δ34.5), glutamine (Gln: C2, δ55; C3, δ27.1; C4, δ31.7), γ-aminobutyric acid (GABA: C2, δ35.3; C3, δ24.5; C4, δ40.2), aspartate (Asp: C2, δ53.2; C3, δ37.5), lactate (Lac: C2, δ69.4; C3, δ21), succinate (Suc: C2/C3, δ35), alanine (Ala: C3, δ17), N-acetyl aspartate (NAA: C2, δ54.1; C3, δ40.5; C6, δ22.8) and taurine (Tau: C1, δ48.3; C2, δ36.2). Furthermore, OPLS-DA based on ^{13}C NMR data was used to discriminate metabolic patterns between APP/PS1 and WT mice at 10 months of age ($R^2Y = 0.755$, $Q^2 = 0.475$). Figure 2c, d illustrates the score and loading plots of OPLS-DA between APP/PS1 and WT mice at 10 months of age, respectively. At 10 months, a clear separation based on ^{13}C NMR data was observed between APP/PS1 and WT mice (Fig. 2c). From its corresponding loading plot, we can see that most signals of ^{13}C-labeled metabolites were higher in WT mice than APP/PS1 mice, as shown in Fig. 2d.

Metabolism of [1-^{13}C]-glucose in the brain of APP/PS1 and WT mice

Metabolism of [1-^{13}C]-glucose in the brain of mice is illustrated in Fig. 3. First of all, [1-^{13}C]-glucose was metabolized to [3-^{13}C]-pyruvate through glycolysis, and then transformed into [3-^{13}C]-Lac by anaerobic glycolysis or [3-^{13}C]-Ala via transamination. In addition, [3-^{13}C]-pyruvate can be converted to [2-^{13}C]-acetyl-CoA by pyruvate dehydrogenase (PDH) in both astrocytes and neurons or [3-^{13}C]-oxaloacetate by pyruvate carboxylase (PC) in astrocytes and then enter the tricarboxylic acid (TCA) cycle. The PC and PDH pathways produce different labeling TCA-derived metabolites. For example, when [3-^{13}C]-pyruvate enters the TCA cycle via the PC pathway, [3-^{13}C]-oxaloacetate and [2-^{13}C]-α-ketoglutarate (α-KG) were labeled, further forming [2-^{13}C]-Glu as well as [2-^{13}C]-Gln. However, from the PDH pathway, [2-^{13}C]-acetyl-CoA and [4-^{13}C]-α-KG were labeled. Then, [4-^{13}C]-α-KG can be further transaminated to [4-^{13}C]-Glu, which is subsequently decarboxylated to [2-^{13}C]-GABA in GABAergic neurons or converted to [4-^{13}C]-Gln in astrocytes. On the second turn of the TCA cycle, the C2 and C3 of Glu, the C2 and C3 of Gln as well as the C3 and C4 of GABA were labeled.

It can be seen from Fig. 3 that APP/PS1 mice had significantly lower ^{13}C labeling from [1-^{13}C]-glucose in all carbon

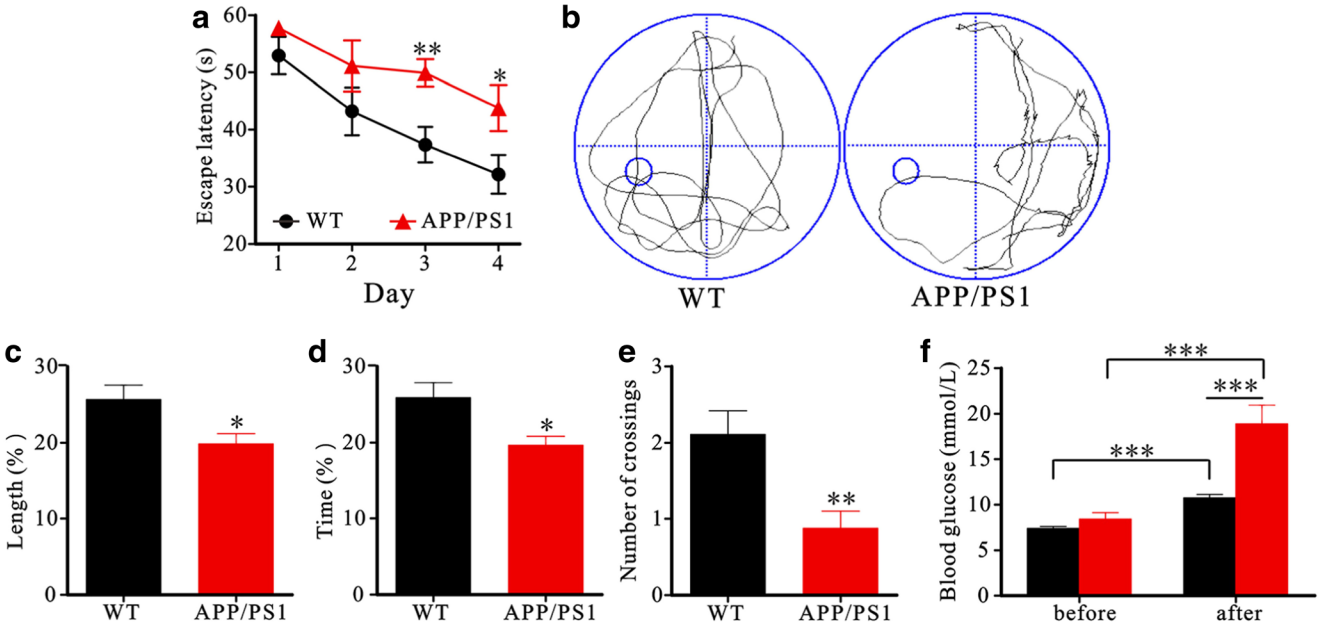

Fig. 1 Spatial learning and memory in wild-type (WT) and APP/PS1 mice assessed by the Morris water maze: **a** escape latency during a 4-day training period; **b** swimming path in the probe test; **c** percentage of swimming length in the target quadrant; **d** percentage of swimming time in the target quadrant; **e** the number of crossings over the original platform location in the probe test; **f** blood glucose level in WT (black bar) and APP/PS1 (red bar) mice before and after intravenous [1-^{13}C]-glucose infusion. Significant level: *P < 0.05; **P < 0.01; ***P < 0.001

positions of Glu (C2, 4.18 ± 0.71 vs. 5.47 ± 0.63, P = 0.005; C3, 3.72 ± 0.53 vs. 5.06 ± 0.58, P = 0.001; C4, 7.53 ± 1.43 vs. 9.76 ± 1.02, P = 0.007) and GABA (C2, 5.08 ± 0.88 vs. 6.66 ± 0.87, P = 0.008; C3, 2.33 ± 0.44 vs. 3.00 ± 0.49, P = 0.025; C4, 2.46 ± 0.61 vs. 3.45 ± 0.52, P = 0.009) than WT mice. Moreover, relative to WT mice, reduced ^{13}C fluxes into all carbon positions of Gln were also detected in APP/PS1 mice, but a significant difference between them was only found in the C3 position (1.87 ± 0.30 vs. 2.27 ± 0.33, P = 0.041). For APP/PS1 mice the ^{13}C-enrichment of Asp was significantly decreased in the C2 (9.31 ± 2.10 vs. 11.82 ± 1.95, P = 0.047) and C3 (7.74 ± 1.36 vs. 10.05 ± 1.35, P = 0.011) positions compared with WT mice. From Fig. 3, we also found that the ^{13}C flux from [1-^{13}C]-glucose into Suc C2/C3 was significantly decreased in APP/PS1 mice relative to WT mice (3.31 ± 1.15 vs. 5.05 ± 0.88, P = 0.01). As compared with WT mice, APP/PS1 mice had a reduction of lactate-alanine shuttle as indicated by decreased ^{13}C fluxes into Ala C3 (4.14 ± 1.22 vs. 6.32 ± 1.24, P = 0.009) as well as Lac C3 (7.73 ± 2.27 vs. 9.97 ± 1.44, P = 0.054). Additionally, it is worth noting that a high level of [1-^{13}C]-glucose can still be observed in the brain of APP/PS1 mice (13.11 ± 8.87), but not detected in WT mice (Fig. 3). Figure 1f also shows that blood glucose level in APP/PS1 mice was significantly higher than that in WT mice after the same amount of [1-^{13}C]-glucose infusion.

Table 1 shows change of metabolite ratio in the brain of WT and APP/PS1 mice after [1-^{13}C]-glucose infusion. We found that the ratios of Glu_{C4}/Gln_{C4} (P = 0.06) and Glu_{C2}/Gln_{C2} (P = 0.01) were lower in the brain of APP/PS1 mice than WT mice. However, as compared with WT mice, $Gln_{C4}/GABA_{C2}$ (P = 0.02) and $Gln_{C2}/GABA_{C4}$ (P = 0.01) ratios were significantly increased in the brain of APP/PS1 mice (Table 1). There were no significant differences between WT and APP/PS1 mice in other metabolic ratios, as shown in Table 1.

Discussion

The main clinical symptoms of AD are spatial learning and memory impairment (Blennow et al. 2006). As expected, the water maze test showed that APP/PS1 mice had an obvious memory and cognitive impairment at 10 months of age in comparison with age-matched WT mice. Brain glucose metabolism has been closely linked to brain function (Mergenthaler et al. 2013; Lauretti et al. 2017; Videbech 2000; Baxter et al. 1989). In the present study, therefore, ^{13}C NMR-based metabolomics in combination with an in vivo injection of [1-^{13}C]-glucose was applied to elucidate glucose metabolism in the brain of APP/PS1 mice at 10 months of age.

Energy metabolism plays a critical role in maintaining normal brain function (Bélanger et al. 2011). It is well known that glucose is an important substance for supplying energy via tricarboxylic acid (TCA) cycle. In the present study, the ^{13}C flux of [1-^{13}C]-glucose into the TCA cycle was detected by ^{13}C NMR spectroscopy as indicated by ^{13}C-labeled Suc, one of key intermediates in the TCA cycle. We found that the ^{13}C-enrichment of Suc C2/C3 was significantly decreased in the brain of APP/PS1 mice at 10 months of age after [1-^{13}C]-

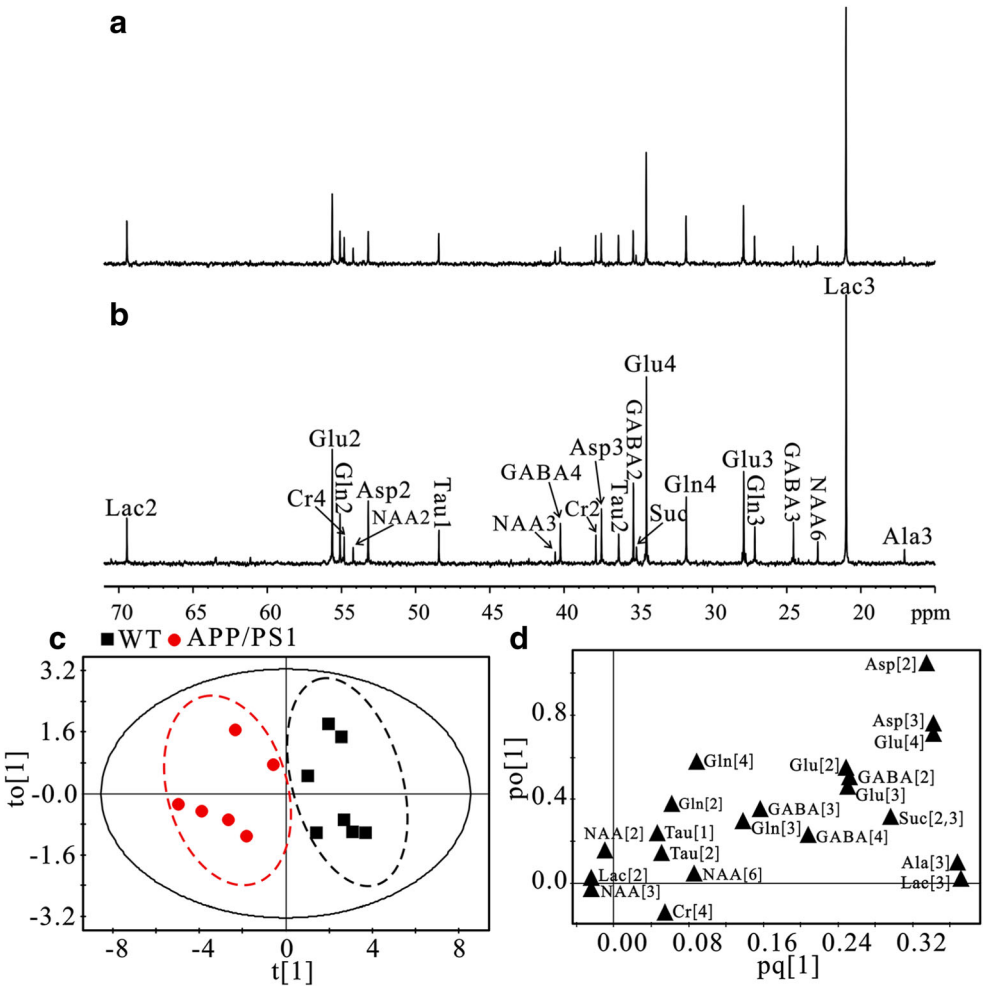

Fig. 2 ^{13}C NMR metabolomic analysis: typical ^{13}C NMR spectra of brain tissue extract in APP/PS1 (**a**) and wild-type (WT, **b**) mice after infused with [1-^{13}C]-glucose; score (**c**) and loading (**d**) plots of OPLS-DA analysis based on ^{13}C NMR data. Metabolite: Ala, alanine; Asp, aspartate; Glu, glutamate; Gln, glutamine; GABA, γ-aminobutyric acid; Lac, lactate; NAA, N-acetyl aspartate; Suc, succinate; Tau, taurine

glucose infusion relative to age-matched WT mice, indicating a reduction of energy metabolism. Interestingly, we also found that glucose was accumulated in the brain of APP/PS1 mice but not in WT mice. These findings indicate a decrease in brain glucose utilization as well as brain energy deficiency during the development of amyloid pathology. One possible explanation could be that the accumulation of amyloid plaques in APP/PS1 mice damaged the mitochondrial function (Xie et al. 2013; Cabezas-Opazo et al. 2015; Anandatheerthavarada et al. 2003). The reduction of brain glucose metabolism has also been reported in AD patient (Mosconi 2005). In our previous study, the ^{13}C-enrichment of Suc C2/C3 was also decreased in the brain of T1D rats at 15 weeks of age after [1-^{13}C]-glucose infusion, indicating a reduced brain energy metabolism (Wang et al. 2015). Furthermore, using ^{13}C NMR technique with intravenous [2-^{13}C]-acetate and [3-^{13}C]-lactate infusions, we found that brain energy metabolism was decreased in astrocytes but not in neurons of T2D mice at 12 weeks of age (Zheng et al. 2017). Taken together, our results suggest that the reduction of brain energy metabolism may be a link between amyloid pathology and diabetic encephalopathy.

Neurotransmitter metabolism is of great importance for maintaining neurotransmitter homeostasis, particularly the Gln-Glu-GABA cycle (Deelchand et al. 2009; Haberg et al. 1998). In astrocytes, Glu is absorbed and synthesized to Gln by glutamine synthetase, which exists predominantly in astrocytes (Norenberg and Martinez-Hernandez 1979). Then, Gln can be transported into neurons and synthesized to Glu by phosphate-activated glutaminase. Moreover, Glu can also be decarboxylated to GABA by glutamic acid decarboxylase in GABAergic neurons. Glu and GABA are the major excitatory inhibitory neurotransmitters in central nervous system, respectively. Therefore, the neurotransmitter shuttling between astrocytes and neurons (so-called the Gln-Glu-GABA cycle) maintains brain neurotransmitter homeostasis. Our results show that the ^{13}C-enrichments of the C2, C3, and C4 of Glu and GABA as well as the C3 of Gln were significantly reduced in the brain of APP/PS1 mice after [1-^{13}C]-glucose infusion as compared with age-matched WT mice. These findings indicate that the Gln-Glu-GABA cycle was down-regulated in the brain of APP/PS1 mice. Moreover, relative to WT mice, the

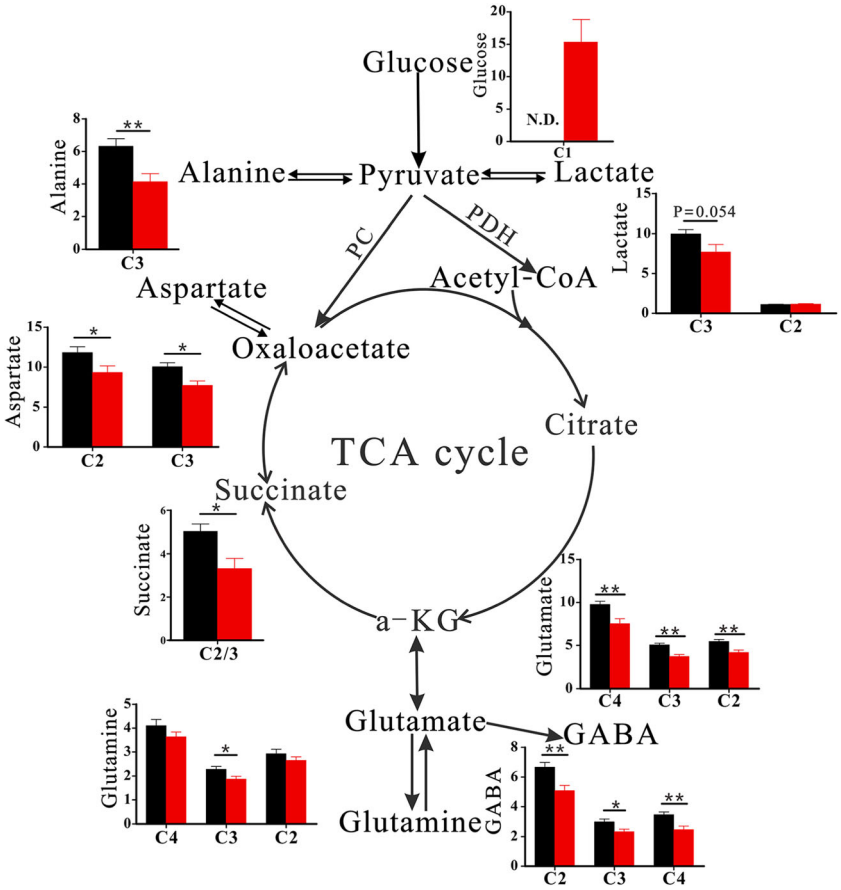

Fig. 3 Brain glucose metabolism in wild-type (WT, black bar) and APP/PS1 (red bar) mice after [1-^{13}C]-glucose infusion. Data are presented as relative enrichment level ± SE; N.D., no detection; Significant level: *$P < 0.05$; **$P < 0.01$

ratio of Glu_{C2}/Gln_{C2} was significantly decreased, while the ratios of $Gln_{C4}/GABA_{C2}$ and $Gln_{C2}/GABA_{C4}$ were significantly increased in the brain of APP/PS1 mice, indicating a decrease in Gln transport from astrocyte to glutamatergic and GABAergic neurons. Previously, we have reported that the conversion of Gln to Glu/GABA was also significantly decreased in 15-week-old T1D rats (Wang et al. 2015) as well as 12-week-old T2D mice (Zheng et al. 2017) by ^{13}C NMR in combination with an in vivo injection of [2-^{13}C]-acetate. Therefore, we speculate that the down-regulation of the Gln-Glu-GABA cycle and the reduction of Gln transport may be common metabolic characteristics between amyloid pathology and diabetic encephalopathy.

Table 1 Change of metabolite ratio in the brain of wild-type (WT) and APP/PS1 mice

Ratio	WT	APP/PS1	P value
Glu_{C4}/Gln_{C4}	2.41 ± 0.22	2.08 ± 0.34	0.06
Glu_{C2}/Gln_{C2}	1.89 ± 0.21	1.58 ± 0.17	0.01
$Glu_{C4}/GABA_{C2}$	1.48 ± 0.16	1.48 ± 0.12	0.95
$Glu_{C2}/GABA_{C4}$	1.60 ± 0.22	1.75 ± 0.31	0.35
$Gln_{C4}/GABA_{C2}$	0.62 ± 0.05	0.72 ± 0.09	0.02
$Gln_{C2}/GABA_{C4}$	0.85 ± 0.09	1.11 ± 0.19	0.01
Glu_{C3}/Glu_{C4}	0.52 ± 0.02	0.50 ± 0.06	0.49
Gln_{C3}/Gln_{C4}	0.56 ± 0.08	0.51 ± 0.05	0.25
Glu_{C2}/Glu_{C4}	0.56 ± 0.03	0.56 ± 0.03	0.83
Gln_{C2}/Gln_{C4}	0.72 ± 0.07	0.73 ± 0.04	0.74

The metabolic ratio was calculated as the ratio of ^{13}C-enrichments between different carbon sites of glutamate (Glu), glutamine (Gln) and γ-aminobutyric acid (GABA), and presented as mean ± SE ($n = 7$)

Asp, as another excitatory neurotransmitter, is derived mainly from oxaloacetate by transamination. In this study, the ^{13}C-enrichments of the C2 and C3 of Asp were significantly lower in the brain of APP/PS1 mice than WT mice after [1-^{13}C]-glucose infusion. This result also reveals a decreased neurotransmitter metabolism in the brain of APP/PS1 mice.

Lactate-alanine shuttle has been reported to regulate the nitrogen exchange between astrocytes and neurons in the brain (Zwingmann et al. 2000; Schousboe et al. 2003; Waagepetersen et al. 2000). However, our results show that the lactate-alanine shuttle was inhibited in the brain of APP/PS1 mice, as indicated by a decrease of ^{13}C flux into Ala C3 and Lac C3 from [1-^{13}C]-glucose. Previously, we also found an identical phenomenon in the brain of 15-week-old T1D rats (Wang et al. 2015). These results indicate that an inhibition of the lactate-alanine shuttle may occur in both amyloid pathology and diabetic encephalopathy.

Conclusions

^{13}C NMR metabolomics combined with intravenous [1-^{13}C]-glucose infusion was conducted to investigate brain glucose metabolism in APP/PS1 mice at 10 month of age. We found that brain glucose utilization was significantly lower in APP/PS1 mice than WT mice, thereby resulting in the reduction of energy and neurotransmitter metabolism. Moreover, we also found that relative to WT mice the lactate-alanine shuttle was inhibited in the brain of APP/PS1 mice. Compared with our previous studies, several common metabolic features may exist in both amyloid pathology and diabetic encephalopathy. In our future work, several suggestions should be considered: (1) brain metabolic rate of glucose can be measured by a multi-time-point ^{13}C-glucose infusion; (2) it could be of great interest to explore glucose metabolic differences between different brain regions; (3) sex difference in the metabolic fate of glucose should be investigate in order to draw the general conclusion; (4) it is important to explore information on gene and protein levels to advance understanding of brain glucose metabolism of amyloid pathology.

Acknowledgments The Laboratory Animal Center of Wenzhou Medical University was appreciated for technical services.

Author contributions HZ and HCG contributed to experimental design. QZ, CL and LCZ contributed to animal feeding and intravenous [1-^{13}C]-glucose infusion, QZ, YD, CL and HHX contributed to sample collection and NMR metabolomic analysis. HZ and HCG contributed to data analysis, result interpretation and writing. All authors have read, revised and approved the final manuscript.

Funding This study was supported by the National Natural Science Foundation of China (Nos.: 21605115, 21575105) and the Public Welfare Technology Application Research Foundation of Zhejiang Province (No.: 2017C33066).

Compliance with ethical standards

Conflicting interests The authors declare no conflict of interest in this study.

References

Anandatheerthavarada HK, Biswas G, Robin MA, Avadhani NG (2003) Mitochondrial targeting and a novel transmembrane arrest of Alzheimer's amyloid precursor protein impairs mitochondrial function in neuronal cells. J Cell Biol 161(1):41–54

Ballarini T, Iaccarino L, Magnani G, Ayakta N, Miller BL, Jagust WJ, Gorno-Tempini ML, Rabinovici GD, Perani D (2016) Neuropsychiatric subsyndromes and brain metabolic network dysfunctions in early onset Alzheimer's disease. Hum Brain Mapp 37(12):4234–4247

Baxter LR, Schwartz JM, Phelps ME, Mazziotta JC, Guze BH, Selin CE, Gerner RH, Sumida RM (1989) Reduction of prefrontal cortex glucose metabolism common to three types of depression. Arch Gen Psychiatry 46(3):243–250

Bélanger M, Allaman I, Magistretti PJ (2011) Brain energy metabolism: focus on astrocyte-neuron metabolic cooperation. Cell Metab 14(6): 724–738

Blennow K, de Leon MJ, Zetterberg H (2006) Alzheimer's disease. Lancet 368(9533):387–403

Cabezas-Opazo FA, Vergara-Pulgar K, Pérez MJ, Jara C, Osorio-Fuentealba C, Quintanilla RA (2015) Mitochondrial dysfunction contributes to the pathogenesis of Alzheimer's disease. Oxid med cell Longev. 2015, Article ID 509654

Deelchand DK, Nelson C, Shestov AA, Ugurbil K, Henry PG (2009) Simultaneous measurement of neuronal and glial metabolism in rat brain in vivo using co-infusion of [1,6-^{13}C2] glucose and [1,2-^{13}C2] acetate. J Magn Reson 196(2):157–163

Ferri CP, Prince M, Brayne C, Brodaty H, Fratiglioni L, Ganguli M, Hall K, Hasegawa K, Hendrie H, Huang Y, Jorm A, Mathers C, Menezes PR, Rimmer E, Scazufca M (2005) Global prevalence of dementia: a Delphi consensus study. Lancet 366(9503):2112–2117

Haberg A, Qu H, Haraldseth O, Unsgard G, Sonnewald U (1998) In vivo injection of [1-^{13}C] glucose and [1,2-^{13}C] acetate combined with ex vivo ^{13}C nuclear magnetic resonance spectroscopy: a novel approach to the study of middle cerebral artery occlusion in the rat. J Cereb Blood Flow Metab 18(11):1223–1232

Hardy J, Selkoe DJ (2002) The amyloid hypothesis of Alzheimer's disease: progress and problems on the road to therapeutics. Science 297(5580):353–356

Holtzman DM, Morris JC, Goate AM (2011) Alzheimer's disease: the challenge of the second century. Sci Transl Med 3(77):77sr1

Hoyer S, Henneberg N, Knapp S, Lannert H, Martin E (1996) Brain glucose metabolism is controlled by amplification and desensitization of the neuronal insulin receptor. Ann N Y Acad Sci 777(1):374–379

Lauretti E, Li JG, Di Meco A, Praticò D (2017) Glucose deficit triggers tau pathology and synaptic dysfunction in a tauopathy mouse model. Transl Psychiatry 7(1):e1020

Li XY, Men WW, Zhu H, Lei JF, Zuo FX, Wang ZJ, Zhu ZH, Bao XJ, Wang RZ (2016) Age- and brain region-specific changes of glucose metabolic disorder, learning, and memory dysfunction in early Alzheimer's disease assessed in APP/PS1 transgenic mice using ^{18}F-FDG-PET. Int J Mol Sci 17(10):1707

Mergenthaler P, Lindauer U, Dienel GA, Meisel A (2013) Sugar for the brain: the role of glucose in physiological and pathological brain function. Trends Neurosci 36(10):587–597

Mosconi L (2005) Brain glucose metabolism in the early and specific diagnosis of Alzheimer's disease. Eur J Nucl Med Mol Imaging 32(4):486–510

Norenberg MD, Martinez-Hernandez A (1979) Fine structural localization of glutamine synthetase in astrocytes of rat brain. Brain Res 161(2):303–310

Saint-Aubert L, Almkvist O, Chiotis K, Almeida R, Wall A, Nordberg A (2016) Regional tau deposition measured by [^{18}F] THK5317 positron emission tomography is associated to cognition via glucose metabolism in Alzheimer's disease. Alzheimers Res Ther 8(1):38

Schousboe A, Sonnewald U, Waagepetersen HS (2003) Differential roles of alanine in GABAergic and glutamatergic neurons. Neurochem Int 43(4):311–315

Shulman GI, Rothman DL, Jue T, Stein P, DeFronzo RA, Shulman RG (1990) Quantitation of muscle glycogen synthesis in normal subjects and subjects with non-insulin-dependent diabetes by ^{13}C nuclear magnetic resonance spectroscopy. N Engl J Med 322(4):223–228

Sibson NR, Mason GF, Shen J, Cline GW, Herskovits AZ, Wall JE, Behar KL, Rothman DL, Shulman RG (2001) In vivo ^{13}C NMR measurement of neurotransmitter glutamate cycling, anaplerosis and TCA cycle flux in rat brain during. J Neurochem 76(4):975–989

Suzanne M (2014) Type 3 diabetes is sporadic Alzheimer′ s disease: mini-review. Eur Neuropsychopharmacol 24(12):1954–1960

Videbech P (2000) PET measurements of brain glucose metabolism and blood flow in major depressive disorder: a critical review. Acta Psychiatr Scand 101(1):11–20

Waagepetersen HS, Sonnewald U, Larsson OM, Schousboe A (2000) A possible role of alanine for ammonia transfer between astrocytes and glutamatergic neurons. J Neurochem 75(2):471–479

Wang N, Zhao LC, Zheng YQ, Dong MJ, Su Y, Chen WJ, Hu ZL, Yang YJ, Gao HC (2015) Alteration of interaction between astrocytes and neurons in different stages of diabetes: a nuclear magnetic resonance study using [1-^{13}C] glucose and [2-^{13}C] acetate. Mol Neurobiol 51(3):843–852

Winkler EA, Nishida Y, Sagare AP, Rege SV, Bell RD, Perlmutter D, Sengillo JD, Hillman S, Kong P, Nelson AR, Sullivan JS, Zhao Z, Meiselman HJ, Wenby RB, Soto J, Abel ED, Makshanoff J, Zuniga E, De Vivo DC, Zlokovic BV (2015) GLUT1 reductions exacerbate Alzheimer's disease vasculo-neuronal dysfunction and degeneration. Nat Neurosci 18(4):521–530

Xie H, Guan J, Borrelli LA, Xu J, Serrano-Pozo A, Bacskai BJ (2013) Mitochondrial alterations near amyloid plaques in an Alzheimer's disease mouse model. J Neurosci 33(43):17042–17051

Zheng H, Zheng Y, Wang D, Cai A, Lin Q, Zhao L, Chen M, Deng M, Ye X, Gao H (2017) Analysis of neuron-astrocyte metabolic cooperation in the brain of db/db mice with cognitive decline using ^{13}C NMR spectroscopy. J Cereb Blood Flow Metab 37(1):332–343

Zwingmann C, Richter-Landsberg C, Brand A, Leibfritz D (2000) NMR spectroscopic study on the metabolic fate of [3-^{13}C] alanine in astrocytes, neurons and cocultures. Glia 32(3):286–303

Zwingmann C, Chatauret N, Leibfritz D, Butterworth RF (2003) Selective increase of brain lactate synthesis in experimental acute liver failure: results of a [^{1}H-^{13}C] nuclear magnetic resonance study. Hepatology 37(2):420–428